

Microphone Utility Estimation in Acoustic Sensor Networks using Single-Channel Signal Features

Michael Günther, Andreas Brendel, *Student Member, IEEE*, and Walter Kellermann, *Fellow, IEEE*

Abstract—In multichannel signal processing with distributed sensors, choosing the optimal subset of observed sensor signals to be exploited is crucial in order to maximize algorithmic performance and reduce computational load, ideally both at the same time. In the acoustic domain, signal cross-correlation is a natural choice to quantify the usefulness of microphone signals, i. e., microphone utility, for array processing, but its estimation requires that the uncoded signals are synchronized and transmitted between nodes. In resource-constrained environments like acoustic sensor networks, low data transmission rates often make transmission of all observed signals to the centralized location infeasible, thus discouraging direct estimation of signal cross-correlation. Instead, we employ characteristic features of the recorded signals to estimate the usefulness of individual microphone signals. In this contribution, we provide a comprehensive analysis of model-based microphone utility estimation approaches that use signal features and, as an alternative, also propose machine learning-based estimation methods that identify optimal sensor signal utility features. The performance of both approaches is validated experimentally using both simulated and recorded acoustic data, comprising a variety of realistic and practically relevant acoustic scenarios including moving and static sources.

Index Terms—channel selection, graph partitioning, microphone utility, acoustic sensor network

I. INTRODUCTION

AN Acoustic Sensor Network (ASN) comprises multiple spatially distributed microphones that typically communicate wirelessly. Capturing different perspectives of the acoustic scene, the signals recorded by these distributed microphones encode spatial information exploitable by multichannel signal processing algorithms. These algorithms accomplish crucial tasks [1] like acoustic source localization [2]–[4] and tracking [5], [6], extraction and enhancement of an acoustic Source of Interest (SOI) [7]–[9], hands-free communication [10], acoustic monitoring [11], [12], as well as scene classification and acoustic event detection [13]. As the microphones in ASNs often have no common sampling

This work was funded by the Deutsche Forschungsgemeinschaft (DFG, German Research Foundation) – 282835863 – within the Research Unit FOR2457 “Acoustic Sensor Networks”.

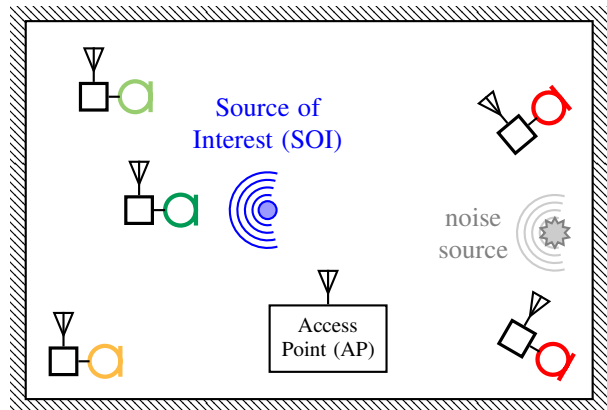


Fig. 1: Scenario for an Acoustic Sensor Network (ASN) with a single SOI captured by spatially distributed microphones.

clock, their signals must be synchronized before joint processing.

The performance of these signal processing algorithms is affected by many factors including the proximity of the microphones to desired and undesired acoustic sources, reverberation, additive noise, orientation and occlusion of microphones, among others. As a result, the signals obtained from different microphones are generally not equally useful for the above-mentioned tasks, potentially even detrimental in extreme cases if inappropriate importance is assigned to them. To ensure optimal algorithmic performance at minimum transmission cost and computational cost, a diligent selection which of the observed microphone signals to process and which to discard is crucial in order to avoid unnecessary signal transmission or synchronization efforts. Unsurprisingly, this task has received considerable attention in the literature: the selection of a single best channel for Automatic Speech Recognition (ASR) based on signal features has been explored in [14]. A utility measure specifically for Minimum Mean Square Error (MMSE) signal extraction has been proposed in [15], [16], followed by a distributed version in [17]. Microphone subset selection to minimize communication cost with upper-bounded

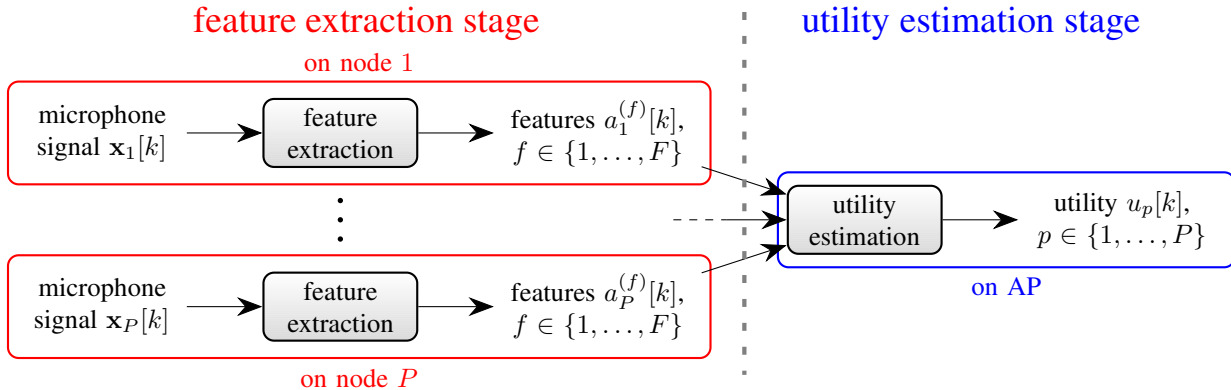


Fig. 2: System overview: In the feature extraction stage, characteristic signal feature sequences are computed for each microphone signal independently. Afterwards, the features sequences from all microphones are collected at the Access Point (AP) and used to estimate each microphone’s utility.

output noise power has been investigated for both Minimum Variance Distortionless Response (MVDR) [18] and Linearly Constrained Minimum Variance (LCMV) [19] beamforming. More recently, joint microphone subset selection and speech enhancement using deep learning was proposed in [20]. However, these methods either neglect the limitations of the underlying ASN regarding communication cost or are tailored to a specific application. In the following, we present a different approach that overcomes both drawbacks, i. e., requires little transmission data rate and is applicable to a broad class of signal processing applications.

Many multichannel algorithms, e. g., for signal enhancement or localization, [7], [21] assume coherent, i. e., linearly related, input signals and exploit the spatial information captured by the inter-channel phase differences. Thus, the cross-correlation of microphone signal pairs and measures derived from it, in particular the spatial coherence and the Magnitude-Squared Coherence (MSC), are intuitive measures for quantifying the usefulness of observed microphone signals and have been used in literature for that purpose, e. g., in [22]. For synchronized microphones with sufficient transmission data rate, direct estimation of the inter-channel coherence from the observed uncoded microphone signals to rate their utility is straightforward. However, in ASNs, this approach is often precluded by a limited transmission data rate, e. g., of current wireless networks [23], especially when the number of microphones is large. This issue is further compounded if the available data rate must be shared with other, possibly non-audio, applications, like video streaming in smart home environments. Furthermore, the microphone signals in ASNs generally do not share a common sampling clock [24], thus requiring potentially costly synchronization prior to estimation of the coherence. Clearly, this disqualifies direct estimation of

the signal cross-correlation as a viable approach for estimating microphone utility in ASNs when promising candidate microphone signals for synchronization and subsequent joint processing should be identified.

Therefore, to address these unique challenges of ASNs, we employ a compressed signal representation in the form of single-channel signal feature sequences, which are extracted from temporal blocks of the microphone signals, to reduce the amount of data to be transmitted. The employed features must be characteristic for the microphone signals, i. e., to allow for (at least approximate) reconstruction of the inter-channel MSC.

In this contribution, we consider acoustic scenarios often encountered in smart home applications comprising a single SOI captured by multiple distributed microphones in an acoustic enclosure, as depicted in Figure 1. After estimating the usefulness of the recorded microphone signals, a subset thereof is selected and transmitted to the central wireless AP for subsequent coherent multichannel signal processing. Although Figure 1 shows an exemplary scenario with a wireless network with a central AP, this is not constraining the scope of the paper. For the considerations in this paper, the network may also be wired and the AP may be replaced by a network node acting as a local center implementing the multichannel signal processing algorithm. Instead of a specific signal processing algorithm, we consider a broad class of algorithms that relies on coherent input signals and does not require signals unrelated to the SOI, e. g., as noise references. In addition, we do not consider application-specific cost functions or performance metrics, e. g., Signal-to-Distortion Ratio (SDR) and Echo Return Loss Enhancement (ERLE), such that the proposed utility estimation scheme is appropriate for many subsequent multichannel signal processing applications. Thus, the proposed generic system takes the form de-

picted in Figure 2 comprising two main subsystems: a feature extraction system, a copy of which runs for each microphone signal on the associated network node, and a utility estimation system running on the AP. In the feature extraction stage, characteristic signal features are extracted from the observed microphone signals independently from each other, i. e., no cross-channel features are employed. The feature sequences obtained from each microphone are then transmitted to the central AP, which estimates the individual microphones' utility values.

In the remainder of this article, we first review and expand model-based realizations of the two subsystems proposed in [25], [26] in Sections III-A and III-B. In Section III-C, we provide new results on the suitability of established signal features for recovering inter-channel MSC. To this end, the feature selection task is formulated as a Least Absolute Shrinkage and Selection Operator (LASSO) regression problem which is then solved numerically to obtain an optimal set of signal features. In Section IV, we propose novel Machine Learning (ML)-based realizations for both subsystems whose combination can be learned in an end-to-end fashion. In Section V, the performance of both model- and ML-based utility estimation approaches is comprehensively validated using experiments on both synthesized and recorded data from realistic scenarios, including different reverberation times, additive noise and obstruction of sensors, different microphone arrangements, as well as static and moving SOIs.

II. NOTATION AND SIGNAL MODEL

In this article, scalar quantities are denoted by slanted non-bold symbols x , while vectors and matrices are denoted by bold-face lowercase \mathbf{x} and uppercase symbols \mathbf{X} , respectively. Furthermore, $[\mathbf{x}]_p$ denotes the p -th element of vector \mathbf{x} , and $[\mathbf{X}]_{p,p'}$ denotes the (p,p') -th element of matrix \mathbf{X} . The J -dimensional all-zeros and all-ones vectors are denoted by $\mathbf{0}_J$ and $\mathbf{1}_J$, respectively, the $J \times J$ identity matrix is denoted by \mathbf{I}_J , and the operator $\text{Diag}(\cdot)$ embeds the elements of its argument on the main diagonal of a square matrix. The Pearson Correlation Coefficient (PCC) of two J -element vectors \mathbf{x} , \mathbf{y} is defined as

$$\mathcal{R}(\mathbf{x}, \mathbf{y}) = \frac{\sum_{j=1}^J ([\mathbf{x}]_j - \bar{x})([\mathbf{y}]_j - \bar{y})}{\sqrt{\sum_{j=1}^J ([\mathbf{x}]_j - \bar{x})^2} \sqrt{\sum_{j=1}^J ([\mathbf{y}]_j - \bar{y})^2}} \quad (1)$$

with means $\bar{x} = \frac{1}{J} \sum_{j=1}^J [\mathbf{x}]_j$ and $\bar{y} = \frac{1}{J} \sum_{j=1}^J [\mathbf{y}]_j$.

In the following, let t denote the discrete-time sample index and let $f \in \{1, \dots, F\}$ denote the feature index where F is the number of extracted features per channel. Recalling Figure 1, we consider an acoustic scenario

comprising a single coherent SOI recorded by P microphones, each of which represents a separate node in the ASN. The signal captured by the microphone indexed by $p \in \mathcal{P} = \{1, \dots, P\}$ is

$$x_p[t] = s[t] * h_p[t] + n_p[t], \quad (2)$$

where $s[t]$ is the dry SOI signal, $h_p[t]$ is the acoustic impulse response from the SOI to the p -th microphone, and $*$ denotes linear convolution. Note that the SOI is not necessarily static, i. e., the acoustic impulse responses $h_p[t]$ in (2) are considered time-invariant only for short observation intervals, but may change from one interval to the next as the SOI moves. The fully coherent spatial images of the SOI $s[t] * h_p[t]$ are superimposed by a spatially diffuse or incoherent noise field, such that the mutual coherence between the noise components $n_p[t]$, $\forall p \in \mathcal{P}$ is negligibly small. Thus, observed correlation between two microphone signals $x_p[t]$, $x_{p'}[t]$ is predominantly caused by the common SOI signal. The signals are partitioned into blocks indexed by $k \in \{1, \dots, K\}$ with a length of L samples and a shift of M between successive blocks, e. g., for the p -th microphone signal $x_p[t]$,

$$\mathbf{x}_p[k] = [x_p[kM], \dots, x_p[kM + L - 1]]^T \in \mathbb{R}^L. \quad (3)$$

As a ground-truth utility measure for the p -th microphone, the frequency-averaged MSC $\gamma_p[k]$ between the (latent) source signal $s[t]$ and the p -th microphone signal $x_p[t]$ is used

$$\gamma_p[k] = \frac{1}{L} \sum_{\nu=1}^L \left| \frac{\Phi_{s,x_p}[k, \nu]}{\sqrt{\Phi_{s,s}[k, \nu] \cdot \Phi_{x_p,x_p}[k, \nu]}} \right|^2, \quad (4)$$

where $\nu \in \{1, \dots, L\}$ denotes the discrete frequency bin index, L is the Discrete Fourier Transform (DFT) length, and $\Phi_{s,x_p}[k, \nu]$, $\Phi_{s,s}[k, \nu]$ and $\Phi_{x_p,x_p}[k, \nu]$ are short-time estimates of the cross-Power Spectral Density (PSD) and auto-PSDs of $s[t]$ and $x_p[k]$, respectively. Under the assumption that the SOI signal $s[t]$ and noise signals $n_p[t]$ are mutually uncorrelated, combined with (2), the relations

$$\Phi_{s,x_p}[k, \nu] = \Phi_{s,s}[k, \nu], \quad (5)$$

$$\Phi_{x_p,x_p}[k, \nu] = \Phi_{s,s}[k, \nu] + \Phi_{n_p,n_p}[k, \nu] \quad (6)$$

hold, such that the summands in (4) simplify to

$$\left| \frac{\Phi_{s,x_p}[k, \nu]}{\sqrt{\Phi_{s,s}[k, \nu] \cdot \Phi_{x_p,x_p}[k, \nu]}} \right|^2 = \frac{\text{SNR}_p[k, \nu]}{\text{SNR}_p[k, \nu] + 1}, \quad (7)$$

with $\text{SNR}[k, \nu] = \frac{\Phi_{s,s}[k, \nu]}{\Phi_{n_p,n_p}[k, \nu]}$. Clearly, the frequency-dependent MSC is a function of the Signal-to-Noise Ratio (SNR), with extremal values $\gamma_p[k, \nu] = 0$ for $\text{SNR}[k, \nu] = 0$, and $\gamma_p[k, \nu] \rightarrow 1$ for $\text{SNR}[k, \nu] \rightarrow \infty$.

The frequency-averaged MSC values of all P microphones are collected in the vector

$$\boldsymbol{\gamma}[k] = [\gamma_1[k], \dots, \gamma_P[k]]^T \in [0, 1]^P. \quad (8)$$

III. MODEL-BASED UTILITY ESTIMATION USING SPECTRAL GRAPH PARTITIONING

We first review the model-based realizations of [25], [26] in Sections III-A and III-B. Advancing the previous heuristic feature selection [27], we formulate the feature selection task as a LASSO regression problem in Section III-C to optimize the trade-off between accuracy and number of features to be transmitted. Solving this problem numerically yields an optimal selection of features for a set of representative acoustic scenarios.

A. Node-wise Feature Extraction

There is a wide variety of potential signal features [28], [29] to describe acoustic signals. Since acoustic scenarios are typically not static in practice due to, e. g., moving acoustic sources or obstructions, the usefulness of microphones is equally time-variant. Hence, within the comprehensive feature taxonomy in [28], we focus on features extracted from short observation intervals to characterize single-channel signals as illustrated in Figure 3. The features may be computed in the time domain based on the digital signal waveform, or in the frequency domain based on the magnitude spectrum of the signals. As a result, we consider the following block-wise features:

- statistical moments (standard deviation, skewness, kurtosis) of the signal waveform
- zero-crossing rate
- statistical moments (standard deviation, skewness, kurtosis) of the magnitude spectrum
- spectral shape features (slope, flatness, roll-off)
- temporal variation of magnitude spectra (spectral flux, spectral variation)

In [27], it was experimentally shown that three features (temporal skewness, temporal kurtosis, spectral flux) are suitable to recover the structure of the spatial MSC matrix of a set of microphone signals. However, the features were selected heuristically based on the visual similarity of the corresponding feature covariance matrices and the ground-truth MSC matrix. Therefore, a more rigorous discussion of the importance of specific signal features is provided in Section III-C.

Generally, a single feature sequence, i. e., a sequence of feature values over several time frames, is insufficient to characterize the signals, since the extraction of each signal feature can at best maintain information about the original signal [30], but typically incurs a loss of information. When multiple sufficiently different features

are used, they capture different parts of the information contained in the signals, such that they complement each other in describing the original signals. Thus, jointly processing such different features allows for a more accurate characterization of the signals compared to a single feature.

To this end, given a signal block $\mathbf{x}_p[k]$, let $a_p^{(f)}[k]$ denote the observed value of the signal feature $f \in \{1, \dots, F\}$ for said signal block. Collecting the feature values of different channels for time frame k yields the instantaneous feature vector

$$\mathbf{a}^{(f)}[k] = [a_1^{(f)}[k], \dots, a_P^{(f)}[k]]^T \in \mathbb{R}^P, \quad (9)$$

which requires only coarse temporal synchronization of the network nodes.

B. Utility Estimation

In this section, we review the utility estimation scheme based on correlation of feature sequences originally proposed in [25]–[27], and show its relation to established Graph Bisection techniques. The model-based utility estimation comprises three steps, which are outlined in the following subsections:

- 1) estimate the cross-channel PCCs of the feature sequences separately for each feature
- 2) fuse information contained in the PCCs from different features
- 3) estimate each microphone's utility from the fused information by means of Spectral Graph Partitioning

For clarity, a visual guide of these steps and the involved matrices and vectors is provided in Figure 4.

Step 1) Feature Correlation Coefficients: For computing the PCCs, first the cross-channel covariance matrices

$$\mathbf{B}^{(f)}[k] = \begin{bmatrix} b_{1,1}^{(f)}[k] & \dots & b_{1,P}^{(f)}[k] \\ \vdots & & \vdots \\ b_{P,1}^{(f)}[k] & \dots & b_{P,P}^{(f)}[k] \end{bmatrix} = \hat{\mathbb{E}} \left(\mathbf{A}^{(f)}[k] \right) \quad (10)$$

are estimated for each feature $f \in \{1, \dots, F\}$ separately. Therein, $\hat{\mathbb{E}}$ denotes an approximate statistical expectation operator whose practical realization we discuss below. Furthermore, the matrix

$$\mathbf{A}^{(f)}[k] = \left(\mathbf{a}^{(f)}[k] - \bar{\mathbf{a}}^{(f)}[k] \right) \left(\mathbf{a}^{(f)}[k] - \bar{\mathbf{a}}^{(f)}[k] \right)^T \quad (11)$$

is the outer product of the instantaneous observed feature vector $\mathbf{a}^{(f)}[k]$ after subtracting its recursive temporal average

$$\bar{\mathbf{a}}^{(f)}[k+1] = \lambda \bar{\mathbf{a}}^{(f)}[k] + (1-\lambda) \mathbf{a}^{(f)}[k+1], \quad (12)$$

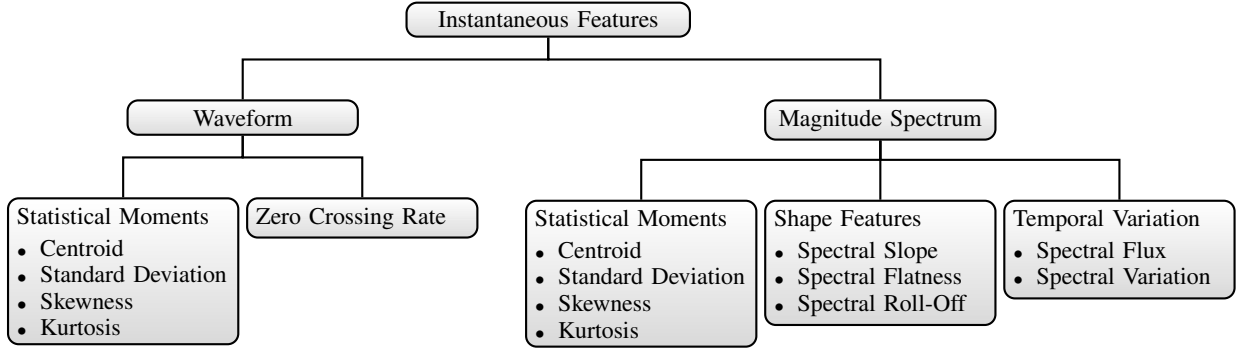


Fig. 3: Feature taxonomy for characterizing microphone signals, adapted from [28].

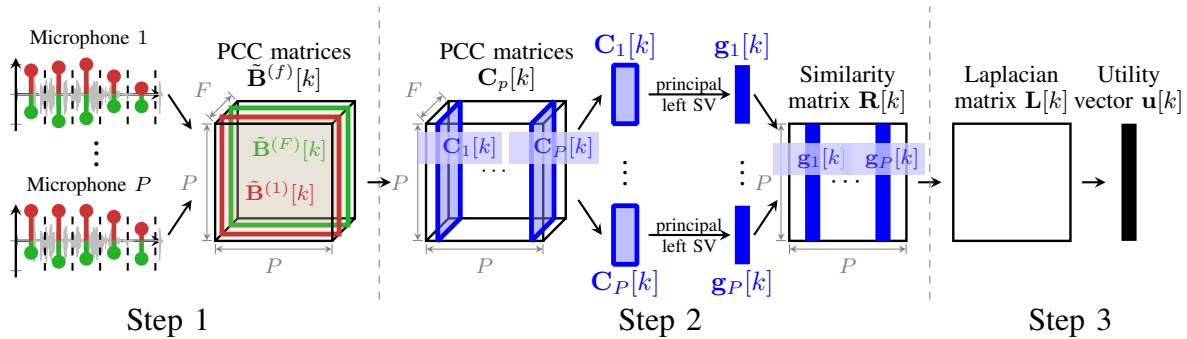


Fig. 4: Overview of model-based utility estimation. For clarity, only two features are illustrated in Step 1.

controlled by the recursive averaging factor $\lambda \in [0, 1]$ with initial value $\bar{\mathbf{a}}^{(f)}[0] = \mathbf{0}_P$.

Note that the estimated $\mathbf{B}^{(f)}[k]$ is generally time-variant to account for the aforementioned SOI movement, and thus online estimation is preferred over batch estimation. In order to track this temporal variability, we use a separate Kalman Filter (KF) [31] for each feature f . Let the latent state vector at time frame k be denoted by $\mathbf{z}^{(f)}[k]$. Its mean vector $\boldsymbol{\mu}^{(f)}[k]$ captures the covariance matrix $\mathbf{B}^{(f)}[k]$ to be estimated and the instantaneous observation vector $\boldsymbol{\xi}^{(f)}[k]$ captures the matrix $\mathbf{A}^{(f)}[k]$. Since both $\mathbf{B}^{(f)}[k]$ and $\mathbf{A}^{(f)}[k]$ are symmetric, it is sufficient to only consider their non-redundant elements. We choose their diagonal elements and lower triangular elements, such that the dimensionality of the state vector $\mathbf{z}^{(f)}[k]$, the mean vector $\boldsymbol{\mu}^{(f)}[k]$ and the observation vector $\boldsymbol{\xi}^{(f)}[k]$ can be chosen to be only $Q = \frac{P(P-1)}{2}$ instead of P^2 while still precisely modeling the full matrices. This can be expressed compactly using the *half-vectorization* operator vech [32], i. e.,

$$\boldsymbol{\mu}^{(f)}[k] = \text{vech} \left(\mathbf{B}^{(f)}[k] \right) \in \mathbb{R}^Q, \quad (13)$$

$$\boldsymbol{\xi}^{(f)}[k] = \text{vech} \left(\mathbf{A}^{(f)}[k] \right) \in \mathbb{R}^Q. \quad (14)$$

Assuming a normally distributed latent state vector $\mathbf{z}^{(f)}[k]$ like in [26] for simplicity and mathematical

tractability leads to the prior distribution

$$p \left(\mathbf{z}^{(f)}[k] \right) = \mathcal{N} \left(\mathbf{z}^{(f)}[k] \mid \boldsymbol{\mu}^{(f)}[k], \mathbf{P}^{(f)}[k] \right) \quad (15)$$

with the aforementioned mean vector $\boldsymbol{\mu}^{(f)}[k]$ and covariance matrix $\mathbf{P}^{(f)}[k] \in \mathbb{R}^{Q \times Q}$. Since the trend of $\mathbf{z}^{(k)}[k]$ is neither known nor easily modelled, we assume a zero-mean Gaussian random walk with transition distribution

$$p \left(\mathbf{z}^{(f)}[k+1] \mid \mathbf{z}^{(f)}[k] \right) = \mathcal{N} \left(\mathbf{z}^{(f)}[k+1] \mid \mathbf{z}^{(f)}[k], \mathbf{S} \right) \quad (16)$$

as it is the least informative model but, due to the Central Limit Theorem (CLT) [33], fits well for natural processes where changes in the latent state are often the result of many independent influences. In order to remain agnostic to the source-microphone arrangement in different scenarios, the time-invariant and feature-independent process noise covariance matrix is chosen as a scaled identity matrix

$$\mathbf{S} = \alpha_1 \mathbf{I}_Q \in \mathbb{R}^{Q \times Q}, \quad (17)$$

where $\alpha_1 \in \mathbb{R}^+$ is a positive tunable parameter. Intuitively, two closely-spaced microphones produce similar feature sequences and thus the way their estimated PCCs w.r.t. to a third microphone change over time will be correlated. While these scenario-specific correlations

could in principle be exploited for more accurate estimation by tailoring \mathbf{S} to the scenario, doing so would harm the generalization of the transition model to other scenarios and furthermore requires the acquisition of sufficient data to estimate an optimal \mathbf{S} . Therefore, to avoid biasing the random walk process, we choose not to model these correlations, i. e., keep \mathbf{S} diagonal.

Choosing, for simplicity, the least informative emission model for the observations $\boldsymbol{\xi}^{(f)}[k]$ for simplicity as well yields the multivariate Gaussian emission distribution

$$p\left(\boldsymbol{\xi}^{(f)}[k] \mid \mathbf{z}^{(f)}[k]\right) = \mathcal{N}\left(\boldsymbol{\xi}^{(f)}[k] \mid \mathbf{z}^{(f)}[k], \mathbf{T}[k]\right) \quad (18)$$

with the observation noise covariance matrix

$$\mathbf{T}[k] = \alpha_2 \left(\text{Diag}\left(\text{vech}\left(\mathbf{E}[k]\right)\right)\right)^{-1} \in \mathbb{R}^{Q \times Q}. \quad (19)$$

Therein, $\alpha_2 \in \mathbb{R}^+$ is a positive tunable parameter and the matrix $\mathbf{E}[k] \in \mathbb{R}^{P \times P}$ contains the geometric means of signal frame energies $e_p[k] = \|\mathbf{x}_p[k]\|_2^2$ (see (3)) reflecting the signal variances for each microphone pair

$$\left[\mathbf{E}[k]\right]_{pp'} = \sqrt{e_p[k] \cdot e_{p'}[k]} + \epsilon, \quad \forall p, p' \in \mathcal{P}. \quad (20)$$

The small positive constant ϵ ensures invertibility of $\mathbf{T}[k]$ in (19) during speech absence periods. This choice is motivated by the notion that the observed feature values are better at characterizing the microphone signals during time frames with high signal energy $e_p[k]$, i. e., the observation noise of the KF is inversely related to the signal energy $e_p[k]$.

With all components of the KF in place, the update equations for mean vector and state covariance are [34]

$$\boldsymbol{\mu}^{(f)}[k+1] = \boldsymbol{\mu}^{(f)}[k] + \mathbf{K}^{(f)}[k] \left(\boldsymbol{\xi}^{(f)}[k] - \boldsymbol{\mu}^{(f)}[k]\right), \quad (21)$$

$$\mathbf{P}^{(f)}[k+1] = \left(\mathbf{P}^{(f)}[k] + \mathbf{S}\right) \left(\mathbf{I}_Q - \mathbf{K}^{(f)}[k]\right), \quad (22)$$

with the Kalman gain matrix

$$\mathbf{K}^{(f)}[k] = \left(\mathbf{P}^{(f)}[k] + \mathbf{S}\right) \left(\mathbf{P}^{(f)}[k] + \mathbf{S} + \mathbf{T}[k]\right)^{-1} \quad (23)$$

and initial values

$$\boldsymbol{\mu}^{(f)}[0] = \mathbf{0}_Q, \quad \mathbf{P}^{(f)}[0] = \mathbf{I}_Q. \quad (24)$$

Note that the updates in (21) to (23) can be computed very efficiently since all involved matrices are diagonal.

For each time frame, after updating the KFs for all features $f \in \{1, \dots, F\}$, the elements of the covariance matrix $\mathbf{B}^{(f)}[k]$ are recovered from the KF mean vector $\boldsymbol{\mu}^{(f)}[k]$ by reversing the half-vectorization, i. e.,

$$b_{p,p'}^{(f)}[k] = \left[\mathbf{B}^{(f)}[k]\right]_{pp'} = \left[\text{vech}^{-1}\left(\boldsymbol{\mu}^{(f)}[k]\right)\right]_{pp'}. \quad (25)$$

Finally, the per-feature cross-channel PCCs as elements of a per-feature PCC matrix $\tilde{\mathbf{B}}^{(f)}[k]$ are obtained

from the estimated covariances by element-wise normalization

$$\tilde{b}_{p,p'}^{(f)}[k] = \left[\tilde{\mathbf{B}}^{(f)}[k]\right]_{pp'} = \frac{b_{p,p'}^{(f)}[k]}{\sqrt{b_{p,p}^{(f)}[k] \cdot b_{p',p'}^{(f)}[k]}}. \quad (26)$$

Step 2) Feature Combination: As outlined earlier, the PCC matrices of different features $\tilde{\mathbf{B}}^{(f)}[k]$ capture different aspects of the underlying inter-channel coherence. To recover an estimate of the inter-channel coherence from the multiple feature correlation coefficient matrices, we consider channel-wise matrices

$$\mathbf{C}_p[k] = \begin{bmatrix} \tilde{b}_{p,1}^{(1)}[k] & \dots & \tilde{b}_{p,1}^{(F)}[k] \\ \vdots & & \vdots \\ \tilde{b}_{p,P}^{(1)}[k] & \dots & \tilde{b}_{p,P}^{(F)}[k] \end{bmatrix} \in \mathbb{R}^{P \times F}, \quad (27)$$

where each $\mathbf{C}_p[k]$ contains the inter-channel PCCs of all F feature sequences of all P microphone channels w. r. t. the corresponding feature sequence of a reference channel p .

Note that each column of $\mathbf{C}_p[k]$, corresponding to one particular signal feature, models the same underlying inter-channel coherence. The PCCs of different features are then combined for each channel p by extracting the dominant column structure of $\mathbf{C}_p[k]$, i. e., finding its best rank-1 approximation in the Least Squares (LS) sense [35]

$$\min_{\sigma_p[k], \mathbf{g}_p[k], \mathbf{h}_p[k]} \left\| \mathbf{C}_p[k] - \sigma_p[k] \mathbf{g}_p[k] \mathbf{h}_p^T[k] \right\|_2^2. \quad (28)$$

Since $\mathbf{C}_p[k]$ is generally non-square, the solution of (28) is obtained by the Singular Value Decomposition (SVD), where $\sigma_p[k] \in \mathbb{R}^+$ is the largest singular value of $\mathbf{C}_p[k]$, and $\mathbf{g}_p[k] \in \mathbb{R}^P$ and $\mathbf{h}_p[k] \in \mathbb{R}^F$ are the principal left and right singular vectors, respectively. The principal left singular vector $\mathbf{g}_p[k]$ captures the contribution of each channel to the dominant structure of $\mathbf{C}_p[k]$, while the principle right singular vector $\mathbf{h}_p[k]$ captures the contribution of each feature to the dominant structure.

To facilitate tracking of $\mathbf{g}_p[k]$ in time-variant scenarios and avoid recomputation of the full SVD in each time step, the principal left singular vector is instead iteratively refined over time. To this end, recall that the left singular vectors of $\mathbf{C}_p[k]$ are identical to the eigenvectors of the Gram matrix $\mathbf{C}_p[k] \mathbf{C}_p^T[k]$ [35]. Thus, given an estimate from the previous time step, the principal singular vector can be estimated using power methods [35] as

$$\check{\mathbf{g}}_p[k+1] = \left(\mathbf{C}_p[k+1] \mathbf{C}_p^T[k+1]\right) \mathbf{g}_p[k], \quad (29)$$

$$\mathbf{g}_p[k+1] = \frac{\check{\mathbf{g}}_p[k+1]}{\|\check{\mathbf{g}}_p[k+1]\|_2}. \quad (30)$$

Note that the spectrum of $\mathbf{C}_p[k]$ varies slowly over time such that a single iteration of (29) and (30) is sufficient.

In order to restore the intuitive notion of a similarity measure, the estimated principal singular vectors from (30) are re-normalized such that the similarity of each channel to itself is equal to one, and then concatenated to form the overall channel similarity matrix

$$\mathbf{R}[k] = \begin{bmatrix} \frac{\mathbf{g}_1[k]}{|\mathbf{g}_1[k]|_1}, & \dots, & \frac{\mathbf{g}_P[k]}{|\mathbf{g}_P[k]|_P} \end{bmatrix} \in \mathbb{R}^{P \times P}. \quad (31)$$

Step 3) Spectral Graph Partitioning: Recalling the signal model in (2), the SOI is assumed to be the only signal component that causes correlation between multiple microphone signals. Thus, microphone selection can be interpreted as partitioning the set of available microphones \mathcal{P} into two, potentially time-variant, disjoint subsets: one set $\mathcal{S}[k]$ whose microphones capture the SOI with high quality and its complement $\bar{\mathcal{S}}[k]$ for microphones dominated by the non-coherent noise field. For a clear distinction of these two groups, an ideal partitioning should exhibit high intra-group similarity and low inter-group similarity, i.e., microphone signals belonging to the same group are similar while microphone signals belonging to different groups are dissimilar. Spectral partitioning techniques operating on graph structures can determine such optimal partitionings very efficiently, especially when the number of microphones P is large. Thus, we model the pairwise similarity of microphone channels using a time-variant graph structure $\mathcal{G}(\mathcal{V}, \mathcal{E}[k])$, comprising a set of vertices \mathcal{V} representing microphones and a set of weighted edges $\mathcal{E}[k]$ representing the microphones' similarity at time frame k . For each edge $(p, p', w_{pp'}[k]) \in \mathcal{E}[k]$, the weight $w_{pp'}[k] \in [0, 1]$ captures the similarity of microphones p and p' . The graph is equivalently specified by its weighted adjacency matrix $\mathbf{W}[k] \in \mathbb{R}^{P \times P}$, containing all weights $w_{pp'}[k], \forall p, p' \in \mathcal{P}$. The pairwise microphone similarity should be a symmetric measure, i.e., channel p should be as similar to p' as channel p' is to p , such that $w_{pp'}[k] = w_{p'p}[k]$. To reflect this symmetry and the varying degrees of similarity, the graph should be undirected and weighted. Since the matrix $\mathbf{R}[k]$ in (31) does not necessarily exhibit these properties, only the symmetric part of its element-wise magnitude is used to construct the weighted adjacency matrix $\mathbf{W}[k]$, i.e.,

$$w_{pp'}[k] = [\mathbf{W}[k]]_{pp'} = \frac{1}{2} \left(\left| [\mathbf{R}[k]]_{pp'} \right| + \left| [\mathbf{R}[k]]_{p'p} \right| \right). \quad (32)$$

The *degree* [36] of the p -th vertex is defined as the sum of all outgoing edges' weights

$$d_p[k] = \sum_{p'=1}^P w_{pp'}[k], \quad (33)$$

which are collected in the diagonal degree matrix

$$\mathbf{D}[k] = \text{Diag} \{d_1[k], \dots, d_P[k]\}. \quad (34)$$

Note that $d_p[k] \geq 1, \forall p \in \mathcal{P}$ since the sum in (33) includes $w_{pp}[k] = 1$, which ensures invertibility of $\mathbf{D}[k]$ even for degenerate graphs.

Now, the graph bisection problem can be formalized as minimization of the inter-group similarity while retaining high intra-group similarity. By keeping the ‘‘size’’ of both sets of the partition reasonable to avoid degenerate solutions, the inter-group and intra-group similarity of a set $\mathcal{S}[k] \subset \mathcal{P}$ and its complement $\bar{\mathcal{S}}[k]$ are measured by [37]

$$\text{cut}(\mathcal{S}[k], \bar{\mathcal{S}}[k]) = \sum_{p \in \mathcal{S}[k], p' \in \bar{\mathcal{S}}[k]} w_{pp'}[k], \quad (35)$$

$$\text{vol}(\mathcal{S}[k]) = \sum_{p \in \mathcal{S}[k]} d_p[k], \quad (36)$$

respectively. Balancing the inter- and intra-group similarity yields the *normalized cut* objective function [38]

$$\text{ncut}(\mathcal{S}[k], \bar{\mathcal{S}}[k]) = \text{cut}(\mathcal{S}[k], \bar{\mathcal{S}}[k]) \cdot \left(\frac{1}{\text{vol}(\mathcal{S}[k])} + \frac{1}{\text{vol}(\bar{\mathcal{S}}[k])} \right). \quad (37)$$

As shown in [38], minimization of (37) w.r.t. \mathcal{S} can be reformulated as minimization of the generalized Rayleigh quotient

$$\min_{\mathcal{S}[k], \bar{\mathcal{S}}[k]} \text{ncut}(\mathcal{S}[k], \bar{\mathcal{S}}[k]) = \min_{\mathbf{y}[k]} \frac{\mathbf{y}^T[k] (\mathbf{D}[k] - \mathbf{W}[k]) \mathbf{y}[k]}{\mathbf{y}^T[k] \mathbf{D}[k] \mathbf{y}[k]}, \quad (38)$$

where $\mathbf{y}[k]$ is a P -dimensional discrete indicator vector satisfying

$$\mathbf{y}^T[k] \mathbf{D}[k] \mathbf{1}_P = 0. \quad (39)$$

Additionally, the elements of $\mathbf{y}[k]$ may only take either of two values [38]

$$[\mathbf{y}[k]]_p \in \left\{ 1, \frac{\sum_{p' \in \mathcal{S}[k]} d_{p'}[k]}{\sum_{p' \in \bar{\mathcal{S}}[k]} d_{p'}[k]} \right\}. \quad (40)$$

When the discreteness constraint (40) on $\mathbf{y}[k]$ is relaxed to allow arbitrary real values, i.e., $\mathbf{y}[k] \in \mathbb{R}^P$, the minimizer of the generalized Rayleigh quotient in (38) is a solution to the generalized eigenvalue problem

$$(\mathbf{D}[k] - \mathbf{W}[k]) \mathbf{y}[k] = \lambda[k] \mathbf{D}[k] \mathbf{y}[k], \quad (41)$$

where $\lambda[k]$ is the generalized eigenvalue and $\mathbf{y}[k]$ is the generalized eigenvector. The equivalent standard eigenvalue problem is obtained by left-multiplication of $\mathbf{D}^{-1}[k]$

$$\mathbf{L}[k] \mathbf{y}[k] = \lambda[k] \mathbf{y}[k] \quad (42)$$

with the normalized random-walk Laplacian matrix [36]

$$\begin{aligned} \mathbf{L}[k] &= \mathbf{D}^{-1}[k] (\mathbf{D}[k] - \mathbf{W}[k]) \\ &= \mathbf{I}_P - \mathbf{D}^{-1}[k] \mathbf{W}[k]. \end{aligned} \quad (43)$$

Thus, an approximate minimizer of (38) is obtained by finding the smallest eigenvalue and its corresponding eigenvector of $\mathbf{L}[k]$. The trivial eigenvalue 0 and its corresponding eigenvector $\mathbf{1}_P$ [37] is excluded by the constraint (39). Thus, the solution is the so-called *Fiedler vector* $\mathbf{v}[k]$, i.e., the eigenvector corresponding to the smallest non-trivial eigenvalue of $\mathbf{L}[k]$ [37], which automatically satisfies (39) as shown in [38]. While an approximate solution to the discrete problem can be obtained by discretizing $\mathbf{v}[k]$, e.g., based on the sign of each element, here we use the real-valued solution directly as an estimate of the microphones' utility.

As an eigenvector, the scale and in particular the sign of $\mathbf{v}[k]$ is ambiguous, i.e., both $-\mathbf{v}[k]$ and $\mathbf{v}[k]$ are valid solutions to the eigenvalue problem (42). The same holds for the objective function (37), which is invariant to exchanging $\mathcal{S}[k]$ with $\overline{\mathcal{S}}[k]$. This ambiguity is usually not a problem for partitioning, since only the association of vertices to groups is desired, but not the identity of each group. In other words, the partitioning given by $\mathbf{v}[k]$ distinguishes between the most and least useful microphones, but does not say which group is which. Additionally, in low-SNR scenarios, noise-dominated microphone signals may exhibit large feature PCC values due to similar noise signal statistics despite only weakly coherent noise signals. To facilitate this distinction, supplemental side information, captured by the vector $\beta[k]$, is correlated with the preliminary utility estimates

$$\rho[k] = \mathcal{R}(\mathbf{v}[k], \beta[k]). \quad (44)$$

Depending on the sign of the Pearson Correlation Coefficient $\rho[k]$, the sign of the estimated utility values is flipped to produce the final utility estimates

$$\mathbf{u}[k] = \begin{cases} \mathbf{v}[k] & \text{if } \rho[k] \geq 0 \\ -\mathbf{v}[k] & \text{if } \rho[k] < 0 \end{cases}. \quad (45)$$

In [25], the supplemental information was chosen as the node degree, i.e., $[\beta[k]]_p = d_p[k]$. While this choice allows detection of outliers if the volumes of the two subsets in the partition are very different, i.e., a large majority of microphones is either useful or not useful, it also requires further assumptions or knowledge about the identity of the majority group, e.g., that the majority of microphones observes the desired SOI. To address these shortcomings, we consider typical SOI and interfering signals: typical SOI signals, like speech, exhibit spectro-temporal structure while typical signal degradations, like reverberation or additive non-coherent noise, reduce said structure. Thus, the differential signal entropy [30]

$$[\beta[k]]_p = -\mathcal{H}(\mathbf{x}_p[k]) \quad (46)$$

capturing the structuredness of signals, was originally used in [26] instead and is used in the following as well.

Algorithm 1 Recursive microphone utility update using Spectral Graph Partitioning

Input: $\mathbf{g}_p[k-1]$, $\forall p \in \mathcal{P}$ (previous similarity vectors)

Input: $b_{p,p'}[k]$, $\forall p, p' \in \mathcal{P}, f \in \{1, \dots, F\}$

Output: $\mathbf{u}[k]$ (estimated utility vector)

for microphones $p = 1$ to P **do**

$\mathbf{g}_p[k] \leftarrow$ updated similarity vector, see (27), (29) and (30)

end for

$\mathbf{R}[k] \leftarrow$ concatenated normalized $\mathbf{g}_p[k]$, $\forall p \in \mathcal{P}$, see (31)

$\mathbf{W}[k] \leftarrow$ symmetric adjacency matrix, see (32)

$\mathbf{L}[k] \leftarrow$ random-walk graph Laplacian, see (43)

$\mathbf{v}[k] \leftarrow$ Fiedler vector of $\mathbf{L}[k]$, see (43)

$\mathbf{u}[k] \leftarrow \pm \mathbf{v}[k]$, after disambiguation (45)

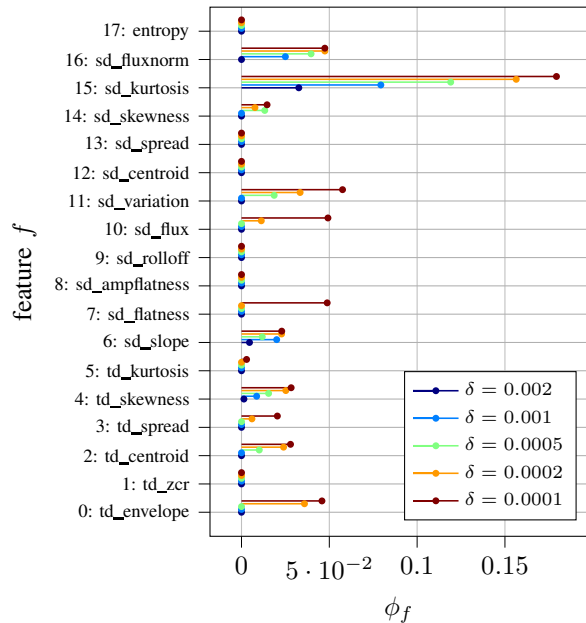


Fig. 5: Feature weights ϕ_f for different values of δ .

Note that, for the experiments conducted in Section V, the signal blocks used to estimate entropy in (46) are chosen longer than those for the feature extraction. The entire microphone utility estimation procedure using Spectral Graph Partitioning is concisely summarized as pseudocode in Algorithm 1.

C. Importance of Specific Signal Features

Choosing an appropriate set of characteristic signal features for the microphone signals is vital: too few features result in low estimation accuracy, while too many features unnecessarily strain the wireless network. Even for an appropriate number of features, inappropriate features may even reduce overall estimation accuracy. To

explore the importance of individual signal features, we cast the feature selection as a LS regression problem with a sparsity-promoting regularizer in order to obtain a low regression error while using as few features as possible. Specifically, we interpret the matrix $\mathbf{C}_p[k]$ as a dictionary matrix whose columns, or *atoms*, contain the cross-channel correlation coefficients between the reference channel p and all channels for one specific signal feature, and which are linearly combined to approximate the MSC of the observed microphone signals. However, for the purpose of estimating microphone utility and microphone selection, the relative utility of microphone channels is more important than the absolute values, such that the zero-mean MSC vector, i. e.,

$$\tilde{\gamma}[k] = \gamma[k] - \left(\frac{1}{P} \sum_{p=1}^P \gamma_p[k] \right) \mathbf{1}_P, \quad (47)$$

is used as the target quantity. Thus, the ℓ_1 -regularized LS cost function for a single acoustic scenario comprising P microphone signals with K time frames is

$$\mathcal{C}(\phi) = \frac{1}{PK} \sum_{p=1}^P \sum_{k=1}^K \|\tilde{\gamma}[k] - \mathbf{C}_p[k]\phi\|_2^2 + \delta \|\phi\|_1, \quad (48)$$

where $\phi = [\phi_1, \dots, \phi_F]^T \in \mathbb{R}^F$ captures the contribution of each feature and the parameter $\delta \in \mathbb{R}^+$ indirectly controls the sparsity of the vector, i. e., the number of used features.

Summing $\mathcal{C}(\phi)$ in (48) over $R_{\text{sim}} = 120$ experiment trials (see Section V-A1) and then minimizing the sum yields the features weights ϕ depicted in Figure 5. Naturally, higher values of δ result in sparser solutions, i. e., less selected features, ranging from 3 features to 12 features for the considered range of δ . The most important features appear to be lower-order statistical moments of the temporal waveform (*td_centroid*, *td_spread*, *td_skewness*), higher-order statistical moments of the magnitude spectrum (*sd_skewness*, *sd_kurtosis*), and features capturing the temporal variation of the magnitude spectrum (*sd_flux*, *sd_variation*, *sd_fluxnorm*). For $\delta = 0.001$, the selection comprises the four features *td_skewness*, *sd_slope*, *sd_kurtosis*, and *sd_fluxnorm*, two of which were part of the informal selection made in [27]. To keep the number of selected features similar to prior work [25], [26], we choose the aforementioned four features of $\delta = 0.001$ for the experimental validation in Section V-B.

IV. LEARNING-BASED UTILITY ESTIMATION

Artificial Neural Networks (ANNs) offer the ability to learn an optimum feature set (for given training data) to characterize the microphone signals, as well as optimally combining the features for estimating microphone utility.

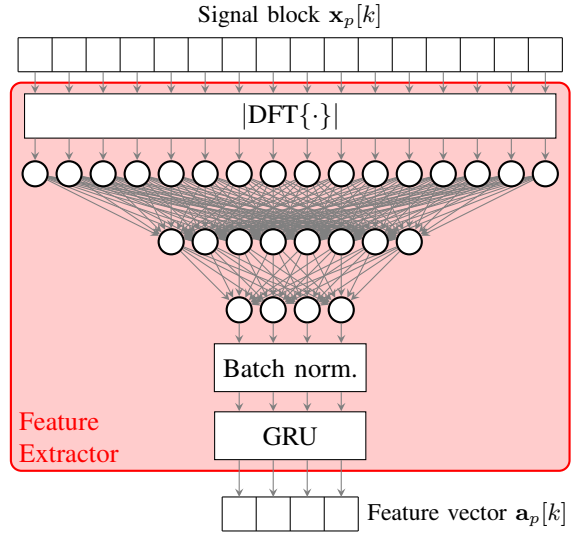


Fig. 6: Architecture of the Feature Extractor module.

Thus, we propose learning-based alternatives to both the model-based feature extraction (see Section III-A) and the utility estimation (see Section III-B) stages. For both stages, network architectures are chosen to reflect the modelling capabilities of their model-based counterparts. Both modules are trained together in an end-to-end fashion. During inference, the extractor and utility estimator modules run on the network nodes and the AP, respectively, such that only the compressed feature representation need to be transmitted to the AP.

A. Node-wise Feature Extraction

The signal features discussed in Section III-C, although effective for utility estimation, are not necessarily optimally suited for utility estimation. Learning a set of features specifically tailored to characterize microphone signals for the purpose of estimating utility promises improved accuracy and a more compact representation. The structure of the feature extractor module is depicted schematically in Figure 6. First, the magnitude spectrum of a single microphone signal block $\mathbf{x}_p[k]$ in (3) is computed. Due to the loss of phase information, this transform is not invertible and thus prevents the model from learning exact equivalents of the time-domain features in Section III-A. However, recalling that the ground-truth utility is given by the MSC, the magnitude spectrum appears to be an obvious choice for the representation of the input data. In addition, models that use magnitude spectrum have outperformed their counterparts that use the time-domain waveform in our experiments. The magnitude spectrum then passes through a series of fully connected feed-forward layers that get progressively narrower until a desired number of signal features is reached.

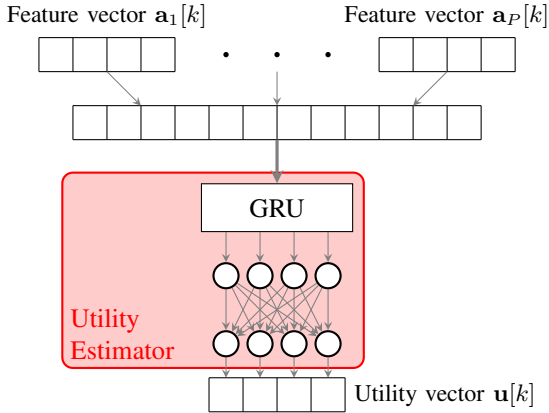


Fig. 7: Architecture of the Utility Estimator module. Feature vectors from different microphones are concatenated to form a single, longer feature vector. The GRUs exploit the temporal information contained in the feature sequences. The FC layers estimate the microphone utility from the GRU outputs.

The final batch normalization and Gated Recurrent Unit (GRU) layer allows the extractor module to learn features that describe the evolution of some quantity over time, e. g., spectral flux. Trained weights are shared between the instances of the module at different microphones, i. e., no sensor-specific features are extracted.

B. Utility Estimation

The architecture of the utility estimator is shown in Figure 7 using the concatenated feature vectors $\mathbf{a}_p[k]$ from the individual microphones as an input. The memory of the first GRU layer allows capturing the temporal evolution of the feature sequences. The following fully connected layers all contain the same number of neurons and are responsible for regression of the GRU outputs onto the target MSC values. Passing in feature sequences directly, as opposed to the PCCs in the model-based method described in Section III, allows the network to differentiate between useful and non-useful microphones, such that no separate disambiguation step or supplemental information is needed. Unlike the model-based estimation in Section III-B, the number of microphones P directly determines the structure of the model which must be retrained when the number of microphones changes.

V. EXPERIMENTAL VALIDATION

The algorithms from Sections III and IV are evaluated on simulated and recorded acoustic data. The considered scenarios feature both static and moving SOIs, different room dimensions and reverberation times, and different arrangements of $P = 10$ microphones, some of which

may be physically obstructed by objects. Estimation accuracy is quantified by computing the time-variant PCC between the estimated utility vector $\mathbf{u}[k]$ and the MSC vector $\boldsymbol{\gamma}[k]$

$$r[k] = \mathcal{R}(\mathbf{u}[k], \boldsymbol{\gamma}[k]). \quad (49)$$

For the following experiments, signals are sampled at $f_s = 16$ kHz. For block processing, signals are partitioned into blocks of $L = 1024$ samples with a block shift of $M = 512$ samples. As the only exception, differential entropy in (46), since it is estimated by a histogram approach, uses longer blocks of 32 000 samples for more robust estimates. Due to the larger block size, the estimated differential entropy also changes more slowly over time, thus promoting temporal continuity of the estimated utility via (45).

For the model-based approach from Section III, termed `model` in the following, the microphone signals are characterized using the four features identified in Section III-C, i. e., `td_skewness`, `sd_slope`, `sd_kurtosis`, and `sd_fluxnorm`. The temporal recursive smoothing factor in (12) is chosen as $\lambda = 0.99$, the scaling factors for the KF process and observation noise are $\alpha_1 = 10^{-4}$ and $\alpha_2 = 0.2$, respectively.

For the learning-based approach, the extractor contains 7 fully connected layers with 513, 256, 128, 64, 32, 16 neurons, respectively, followed by a single GRU layer with 16 inputs and 16 hidden states. Recall that $L = 1024$ such that the 513 inputs to the first layer correspond to the non-redundant part of the signal's magnitude spectrum. The utility estimator contains a single GRU layer with $16P = 160$ inputs and 10 hidden states, followed by 3 fully connected layers with 10 neurons each. Since identical copies of the extractor module are run for each microphone channel $p \in \mathcal{P}$, the total number of parameters is 175 000 for the extractor regardless of the number of microphones P , and 5 500 for the utility estimator with the above configuration which scales asymptotically quadratically with the number of channels P . The objective function to be minimized in training is the Mean Square Error (MSE) between the estimated utility $\mathbf{u}[k]$ and the ground-truth MSC $\boldsymbol{\gamma}[k]$

$$\min_{\Psi} \frac{1}{K} \sum_{k=1}^K \|\mathbf{u}_{\Psi}[k] - \boldsymbol{\gamma}[k]\|_2^2, \quad (50)$$

where Ψ denotes the set of all trainable parameters, trained by the Adam optimizer [39] with a learning rate of 10^{-3} . The model is first trained on simulated data (see Section V-A1) which is split into 70% training and 30% validation data, termed `ML-sim`. To investigate the generalization to unseen data, a copy of the so-trained model is fine-tuned on recorded data, termed `ML-tuned`. Finally, a version trained on both simulated

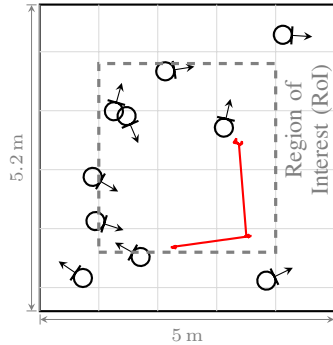


Fig. 8: Simulated room A and exemplary source trajectory (red) for synthesized data.

TABLE I: Dimensions and reverberation times of simulated rooms.

Room	Dimensions			Reverberation Time T_{60}
	x [m]	y [m]	z [m]	
A	5.0	5.2	3.0	500 ms
B	6.2	5.0	2.5	700 ms
C	4.8	4.2	2.3	350 ms

and recorded data simultaneously, termed `ML-joint`, is also evaluated.

A. Acoustic Data

1) *Simulated*: Microphone signals for a single SOI moving in a shoe box room are simulated using the image-source method [40], [41]. Male and female speech segments of 28s duration are used as SOI signals. The source moves rapidly during the time intervals 8s – 10s and 18s – 20s, and otherwise moves slightly around a resting position to simulate the behaviour of human speakers. Under these constraints, 20 different, random source trajectories are generated. Three different rooms with typical living room-like acoustic properties (see Table I) are considered. In each room, $P = 10$ cardioïd microphones are placed at random positions and with random azimuthal rotation. In total, $R_{\text{sim}} = 120$ distinct acoustic setups (20 trajectories \times 2 signals \times 3 rooms) are simulated. The generated source images are superimposed with spatially uncorrelated white noise of equal level to attain an SNR of 10 dB at the microphone with the strongest source image on average, such that other microphones have lower SNRs. Figure 8 illustrates Room A along with an exemplary source trajectory.

2) *Recorded*: The recorded acoustic data is obtained from $P = 10$ microphones arranged pair-wise in a quarter circle around a static loudspeaker representing the SOI as shown in Figure 9. SOI signals comprise male, female and children’s speech. Instead of a moving source, different usefulness of the microphones is induced by occluding some of the sensors. Obstacles may

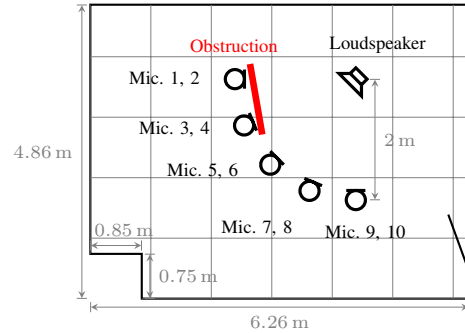


Fig. 9: Experiment setup and exemplary obstruction for recorded data.

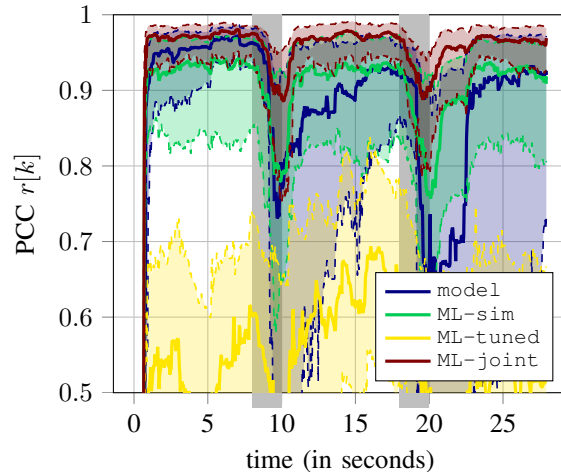


Fig. 10: Median (solid) and lower/upper quartile (dashed) of PCC $r[k]$ over all $R_{\text{sim}} = 120$ synthetic experiment trials. Grey-shaded areas indicate time intervals of source movement.

cover two microphone pairs as indicated in Figure 9, or a single microphone pair. Additionally, obstacles consist of different materials, i. e., solid wood, foam and cloth, such that sound can permeate through some of them. In total, $R_{\text{rec}} = 36$ distinct acoustic setups (12 obstructions \times 3 signals) are recorded. Like for simulated data, spatially uncorrelated white noise is added to the recorded microphone signals to achieve an SNR of 10 dB.

B. Experimental Results

1) *Simulated Data*: Figure 10 shows the median, as well as lower and upper quartile, of the PCC $r[k]$ across trials as a function of the time frame k for simulated data, which should ideally produce values close to 1. Whenever the source moves (indicated by the grey-shaded areas in Figure 10), the source-microphone distances suddenly change causing the observed rapid decrease of $r[k]$. For `model`, breakdowns are quite

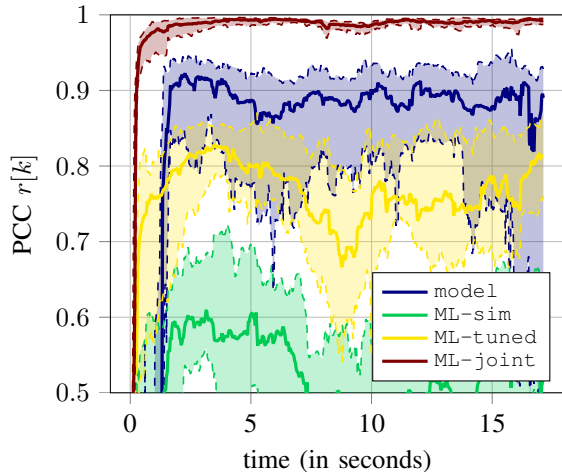


Fig. 11: Median (solid) and lower/upper quartile (dashed) of PCC $r[k]$ over all $R_{\text{rec}} = 36$ real-data experiment trials.

severe and take until the next source movement to recover. Although `ML-sim` does not quite reach the accuracy of `model` during the first 8s, its breakdowns after movement are much less severe and recovery is faster, effectively outperforming `model` after 10s. As expected, fine-tuning the ML model using recorded data significantly degrades performance for simulated data, as shown by `ML-tuned`. Finally, the ML model with both simulated and recorded data from the beginning, i.e., `ML-joint`, clearly outperforms all other considered methods, with only minor breakdowns and very fast recovery. Interestingly, incorporating recorded data besides the simulated into the training procedure also improves performance on simulated data.

While the ML models implicitly learning the temporal structure of the source movement might be a concern here, our experiments with random time intervals of 4s to 12s between source movements have shown no noticeable degradation compared to fixed time intervals.

2) *Recorded Data:* As before, Figure 10 shows the median, as well as lower and upper quartile, of the PCC $r[k]$ across trials as a function of the time frame k for recorded data. Since the SOI is static, the usefulness of microphones is predominantly influenced by their occlusion, no clear temporal structure can be discerned. While the median of `model` is around 0.9, its interquartile distance is quite large. Meanwhile, `ML-sim` only achieves median values of around 0.5, which is unsurprising since the model did not encounter recorded data during training. Even after fine-tuning on recorded data, the performance of `ML-tuned` does not match `model`. Like for simulated data, `ML-joint` also outperforms other methods on recorded data, achieving almost ideal

values extremely fast and consistently, i.e., at almost no spread.

3) *Discussion:* Let us summarize Sections V-B1 and V-B2 and point out implications for practical application. The ML-based approaches, especially `ML-joint`, provide very good utility estimates but require recorded acoustic data for training. For ASNs in realistic conditions, obtaining a sufficient amount of labeled training data is non-trivial since the estimation of the MSC values necessary for training require prior transmission and potentially synchronization of the observed signals. Furthermore, the architecture of the utility estimator module explicitly depends on the number of microphones P and thus requires retraining whenever P changes, e.g., new ASN nodes are added.

In contrast, the model-based approach `model` has shown a more modest, yet robust, performance for both simulated and recorded data. It is also blind, i.e., does not require knowledge of array geometries, acoustic meta parameters like reverberation time, and especially the number of microphones P . Thus, it can be straightforwardly deployed in different acoustic environments with the need to collect acoustic data to train or fine-tune the model. For a real system, a model-based scheme can be used as initial solution to collect labeled training data, which can then be used to tailor an ML-based model to the specific acoustic scenario of the training data.

VI. CONCLUSION

In this contribution, we tackled microphone utility estimation for ASNs. Specifically, we revisited model-based approaches and discussed the usefulness of specific features, with features describing temporal variations and higher-order statistical moments of the signals' magnitude spectra being the most useful overall. Furthermore, we proposed alternative, machine learning-based realizations to learn an optimal feature set and utility estimator. Experimental validation showed that both model- and ML-based approaches are viable in principle with their own strengths and drawbacks. The model-based approach is straightforwardly applied to ASNs with an arbitrary number of microphones P , but is clearly outperformed by suitably trained ML models. In contrast, the ML-based approaches, particularly `ML-joint`, achieve excellent performance if matching training data are available.

REFERENCES

- [1] A. Bertrand, "Applications and trends in wireless acoustic sensor networks: A signal processing perspective," in *2011 18th IEEE Symposium on Communications and Vehicular Technology in the Benelux (SCVT)*, Nov. 2011, pp. 1–6.
- [2] H. Wang and P. Chu, "Voice source localization for automatic camera pointing system in videoconferencing," in *1997 IEEE International Conference on Acoustics, Speech, and Signal Processing*, vol. 1, Apr. 1997, pp. 187–190.

- [3] L. Cheng, C. Wu, Y. Zhang, H. Wu, M. Li, and C. Maple, "A Survey of Localization in Wireless Sensor Network," *International Journal of Distributed Sensor Networks*, vol. 8, no. 12, Dec. 2012.
- [4] A. Brendel and W. Kellermann, "Distributed source localization in acoustic sensor networks using the coherent-to-diffuse power ratio," *IEEE Journal of Selected Topics in Signal Processing*, vol. 13, no. 1, pp. 61–75, 2019.
- [5] L. Kaplan, Q. Le, and N. Molnar, "Maximum likelihood methods for bearings-only target localization," in *IEEE Int. Conf. Acoust., Speech, Signal Process. (ICASSP)*, May 2001, pp. 3001–3004 vol.5.
- [6] C. Evers, H. W. Löllmann, H. Mellmann, A. Schmidt, H. Barfuss, P. A. Naylor, and W. Kellermann, "The LOCATA challenge: Acoustic source localization and tracking," *IEEE/ACM Transactions on Audio, Speech, and Language Processing*, vol. 28, pp. 1620–1643, 2020.
- [7] M. Brandstein, *Microphone arrays: signal processing techniques and applications*. Springer Science & Business Media, 2001.
- [8] A. Bertrand and M. Moonen, "Distributed adaptive estimation of correlated node-specific signals in a fully connected sensor network," in *IEEE Int. Conf. Acoust., Speech, Signal Process. (ICASSP)*, Taipei, Taiwan, Apr. 2009, pp. 2053–2056.
- [9] S. Markovich-Golan, A. Bertrand, M. Moonen, and S. Gannot, "Optimal distributed minimum-variance beamforming approaches for speech enhancement in wireless acoustic sensor networks," *Signal Processing*, vol. 107, pp. 4–20, 2015.
- [10] S. L. Gay and J. Benesty, *Acoustic signal processing for telecommunication*. Springer Science & Business Media, 2012, vol. 551.
- [11] L. M. Oliveira and J. J. Rodrigues, "Wireless Sensor Networks: a Survey on Environmental Monitoring," *Journal of Communications*, vol. 6, no. 2, pp. 143–151, Apr. 2011.
- [12] S. Goetze, J. Schroder, S. Gerlach, D. Hollosi, J.-E. Appell, and F. Wallhoff, "Acoustic monitoring and localization for social care," *Journal of Computing Science and Engineering*, vol. 6, no. 1, pp. 40–50, 2012.
- [13] A. Mesaros, T. Heittola, A. Diment, B. Elizalde, A. Shah, E. Vincent, B. Raj, and T. Virtanen, "DCASE 2017 Challenge setup: Tasks, datasets and baseline system," in *DCASE 2017 - Workshop on Detection and Classification of Acoustic Scenes and Events*, Munich, Germany, Nov. 2017. [Online]. Available: <https://hal.inria.fr/hal-01627981>
- [14] M. Wolf and C. Nadeu, "Towards microphone selection based on room impulse response energy-related measures," in *Proc. of I Joint SIG-IL/Microsoft Workshop Speech Lang. Technol. Iberian Lang.*, Porto Salvo, Portugal, 2009, p. 4.
- [15] A. Bertrand and M. Moonen, "Efficient sensor subset selection and link failure response for linear MMSE signal estimation in wireless sensor networks," in *European Signal Process. Conf. (EUSIPCO)*, Aalborg, Denmark, Aug. 2010, pp. 1092–1096.
- [16] J. Szurley, A. Bertrand, M. Moonen, P. Ruckebusch, and I. Moerman, "Energy aware greedy subset selection for speech enhancement in wireless acoustic sensor networks," in *European Signal Process. Conf. (EUSIPCO)*, Aug. 2012, pp. 789–793.
- [17] J. Szurley, A. Bertrand, P. Ruckebusch, I. Moerman, and M. Moonen, "Greedy distributed node selection for node-specific signal estimation in wireless sensor networks," *Signal Processing*, vol. 94, pp. 57–73, Jan. 2014.
- [18] J. Zhang, S. P. Chepuri, R. C. Hendriks, and R. Heusdens, "Microphone Subset Selection for MVDR Beamformer Based Noise Reduction," *IEEE/ACM Transactions on Audio, Speech, and Language Processing*, vol. 26, no. 3, pp. 550–563, Mar. 2018.
- [19] J. Zhang, J. Du, and L.-R. Dai, "Sensor Selection for Relative Acoustic Transfer Function Steered Linearly-Constrained Beamformers," *IEEE/ACM Transactions on Audio, Speech, and Language Processing*, vol. 29, 2021.
- [20] J. Casebeer, J. Kaikaus, and P. Smaragdis, "Communication-Cost Aware Microphone Selection for Neural Speech Enhancement with Ad-Hoc Microphone Arrays," in *IEEE Int. Conf. Acoust., Speech, Signal Process. (ICASSP)*, Jun. 2021, pp. 8438–8442.
- [21] J. Benesty, J. Chen, and Y. Huang, *Microphone array signal processing*. Springer Science & Business Media, 2008, vol. 1.
- [22] K. Kumatani, J. McDonough, J. Lehman, and B. Raj, "Channel selection based on multichannel cross-correlation coefficients for distant speech recognition," in *Joint Workshop Hands-free Speech Commun. Microphone Arrays (HSCMA)*, Edinburgh, UK, May 2011, pp. 1–6.
- [23] "IEEE Standard for Information technology – Telecommunications and information exchange between systems Local and metropolitan area networks - Specific requirements - Part 11: Wireless LAN Medium Access Control (MAC) and Physical Layer (PHY) Specifications," *IEEE Std 802.11-2016 (Revision of IEEE Std 802.11-2012)*, pp. 1–3534, 2016.
- [24] A. Chinaev, G. Enzner, T. Gburrek, and J. Schmalenstroer, "Online Estimation of Sampling Rate Offsets in Wireless Acoustic Sensor Networks with Packet Loss," in *European Signal Process. Conf. (EUSIPCO)*, 2021, pp. 1–5.
- [25] M. Günther, H. Afifi, A. Brendel, H. Karl, and W. Kellermann, "Network-aware optimal microphone channel selection in wireless acoustic sensor networks," in *IEEE Int. Conf. Acoust., Speech, Signal Process. (ICASSP)*, Jun. 2021.
- [26] M. Günther, A. Brendel, and W. Kellermann, "Online estimation of time-variant microphone utility in wireless acoustic sensor networks using single-channel signal features," in *European Signal Process. Conf. (EUSIPCO)*, Dublin, Ireland, 2021.
- [27] —, "Single-channel signal features for estimating microphone utility for coherent signal processing," in *Int. Congress on Acoust. (ICA)*, Sep. 2019, pp. 2716–2723.
- [28] G. Peeters, "A large set of audio features for sound description (similarity and classification)," *CUIDADO project Ircam technical report*, 2004. [Online]. Available: http://recherche.ircam.fr/equipements/analyse-synthese/peeters/ARTICLES/Peeters_2003_cu
- [29] T. Virtanen, M. Plumbley, and D. Ellis, *Computational analysis of sound scenes and events*. Springer, 2018.
- [30] T. M. Cover and J. A. Thomas, *Elements of information theory*, 2nd ed. Hoboken, N.J: Wiley-Interscience, 2006.
- [31] R. E. Kalman, "A New Approach to Linear Filtering and Prediction Problems," *Journal of Basic Engineering*, vol. 82, no. 1, pp. 35–45, Mar. 1960. [Online]. Available: <https://doi.org/10.1115/1.3662552>
- [32] H. V. Henderson and S. R. Searle, "Vec and vech operators for matrices, with some uses in Jacobians and multivariate statistics," *Canadian Journal of Statistics*, vol. 7, no. 1, pp. 65–81, 1979.
- [33] A. Papoulis and S. U. Pillai, *Probability, Random Variables and Stochastic Processes*, 4th ed. McGraw-Hill, 2001.
- [34] C. M. Bishop, *Pattern Recognition and Machine Learning*. Springer, 2006.
- [35] G. H. Golub and C. F. Van Loan, *Matrix Computations*, 3rd ed. The Johns Hopkins University Press, 2013.
- [36] F. R. Chung and F. C. Graham, *Spectral graph theory*. American Mathematical Soc., 1997, no. 92.
- [37] U. Von Luxburg, "A tutorial on spectral clustering," *Statistics and computing*, vol. 17, no. 4, pp. 395–416, 2007.
- [38] J. Shi and J. Malik, "Normalized cuts and image segmentation," *IEEE Transactions on Pattern Analysis and Machine Intelligence*, vol. 22, no. 8, pp. 888–905, Aug. 2000.
- [39] D. P. Kingma and J. Ba, "Adam: A Method for Stochastic Optimization," 2017.
- [40] J. B. Allen and D. A. Berkley, "Image method for efficiently simulating small-room acoustics," *The Journal of the Acoustical Society of America*, vol. 65, no. 4, pp. 943–950, 1979.
- [41] E. A. P. Habets, "Signal generator for MATLAB," Sep. 2011. [Online]. Available: <https://github.com/ehabets/Signal-Generator>